A Three-Dimensional Parametric Study of the Effects of a Fault Rupture on a Multi-Story Building

Dildar Ali Mangnejo
Department of Civil Engineering, Mehran University, Pakistan
dildarali@muetkhp.edu.pk
(corresponding author)

Israr Ahmed Channa
Department of Civil Engineering, Quaid-e-Awam University of Engineering, Science & Technology, Pakistan
israrchanna8@gmail.com

Muhammad Auchar Zardari
Department of Civil Engineering, Quaid-e-Awam University of Engineering, Science & Technology, Pakistan
muhammad.auchar@quest.edu.pk

Received: 4 January 2023 | Revised: 21 January 2023 | Accepted: 23 January 2023

ABSTRACT

Earthquake events have shown that besides the earthquake forces, the interaction between the fault rupture and structures could cause a lot of damage. Field observations have revealed the need to design structures for fault-induced loading in regions with active faults. In this study, three-dimensional numerical simulation was carried out to evaluate the performance of a 20-story frame building subjected to the propagation of normal fault rupture. A parametric study was conducted with the propagation of the fault slip (h) with outcrop to the right (s/B=-1.0), at the mid (s/B=0.5), and left (s/B=2.0) of the raft. An advanced hypoplastic sand model (which can capture small-strain stiffness and stress-state dependent dilatancy of sand) was adopted. The Concrete Damaged Plasticity (CDP) model was used to capture the cracking behavior in the concrete beams, columns, and piles. The computed results revealed that the performance of the building due to the propagation of the normal fault rupture depends on the position of the outcrop of the rupture with respect to the building. Among the three simulated cases, the maximum differential settlement occurred when s/B= 0.5. In each case, the lateral movement of the building caused inter-story drift which may induce distress in the structural components of the building. The beams and the columns of the first story were fully damaged in tension when s/B was equal to -1.0 or 0.5.

Keywords-high-rise building; normal fault rupture; differential settlement; damage

I. INTRODUCTION

High-rise buildings are often planned in areas with intensive active faults [1]. Faults are lengthy areas where the layers of the ground are fractured and produce a zone. These fractures are often slant and are not vertical. Thus, it has become important to investigate the effects of fault rupture causing damage to the infrastructure [2]. With surface rupture there are many unknowns, so a probabilistic analysis is currently the best approach for the development of a range of expected displacements. However, the actual displacement that occurs with surface rupture can vary drastically from the expected values. To understand the failure mechanism of these foundation systems, including strip and caisson foundations, experimental and theoretical studies have been conducted [3-8]. The position of the foundation relative to the bedrock fault and the magnitude of the bedrock fault movement were found to be crucial influencing factors. In addition, the presence of foundation systems modifies the path of fault ruptures, as the latter propagates from the bedrock to the ground surface. Pile foundations, as deep foundations, behave differently from shallow ones when subjected to faulting-induced deformation [3, 9]. In some specific cases [10], ground movement after an earthquake reportedly caused cracks and deformation of pile foundations. The mechanism behind this type of failure is significant for the performance of structures. Researchers have

recently developed theoretical methods to evaluate the behavior of piles subjected to soil movement induced by normal faults [5]. Although the main characteristics of fault-rupture propagation can be well described by advanced constitutive models, physical modeling is necessary to derive deeper insight into the interaction mechanisms and to offer experimental data for model validation. In addition, very limited field data are available to verify the theoretical methods because it is practically impossible to simulate a bedrock fault movement in the field. Among those numerical studies, however, responses of framed building to excavation were reported in some. However, most of the previous studies have focused on the fault effects on shallow foundations. Therefore, there is a gap of systematic research on the response of a high-rise building subjected to live load and resting on piled raft to the propagation of a normal fault rupture outcrop at different distances from the building. To obtain a satisfactory numerical model of twin excavation effects on high-rise buildings, the analysis needs to take into account the small strain non-linearity of the soil. In view of the aforementioned issues, this study aims to systematically investigate the effects of a normal fault rupture on an existing 20-story high rise building in sand. To achieve these objectives, three-dimensional finite element analysis was conducted.

II. CHARACTERISTICS OF A SOIL-PILE-STRUCTURE SYSTEM

A. General

With the prime objective of investigating the effects of propagation of normal fault rupture on a high-rise building, three-dimensional finite element analysis was adopted in this study. A normal rupture with dip angle of 60^0 was imposed at the proximity of a 20-story high-rise building which is resting on a 4×4 piled raft foundation in sand (with relative density, D_r=70%). Figure 1(a) illustrates the general setup of the 20-story building founded on the piled raft.

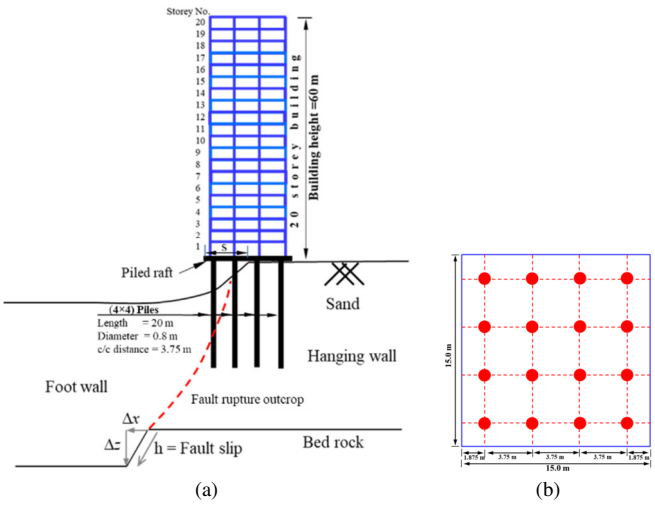

(a) (b)

Fig. 1. (a) Schematic illustration of a normal fault rupture interaction with a high-rise building, (b) piles arrangement in the raft.

A 60m high, 15m wide 20-story concrete building with 3 spans in each direction was selected in study. The building was founded on a square raft, 15m wide and 1.5m thick, supported by a group of piles in a 4×4 configuration with center-to-center distance of 3.75m (see Figure 1(b)). The diameter (d_p) and the length (L_p) of each pile were 1m and 20m, respectively. A normal rupture (having length of fault slip h=60cm) with dip angle of 60^0 with the horizontal was imposed at the proximity of the building. The prime objective of this study is to assess the impact of normal fault rupture on the 20-story building under dead and live loads. A live load of 5kPa was adopted in this study. With this adopted piled raft system, the numerical prediction showed that settlement of the building due to dead and live load was 8mm (0.8% dp) which is within the limit of the allowable foundation settlement of 50mm [11]. The parametric study was conducted with propagation of the fault slip (h) with an outcrop to the right (s/B=−1.0), at the mid (s/B=0.5), and the left (s/B=2.0) of the piled raft (where s is the distance between the left edge of the raft and the emergence of the fault at ground surface and B is the width of the raft).

B. Features of the Building

Figure 2(a) shows the sections (with reinforcement details) of a typical beam and column of the high-rise building. The sections were designed by a routine design procedure using SAP2000 based on ACI. All the sections of the beams and columns are rectangular in shape having sizes of 230mm by 600mm and 230mm by 460mm, respectively. Each beam is reinforced with tension and compression steel bars. Tension and compression reinforcement consist of three 12mm diameter bars and three 12mm diameter bars, respectively. The bars have 60mm center to center spacing. These main bars are confined by 10mm diameter stirrups with center to center spacing of 125mm. Each column is reinforced with six 12 mm diameter main bars. These main bars are confined by the lateral ties having diameter 10mm at center to center spacing of 150mm.

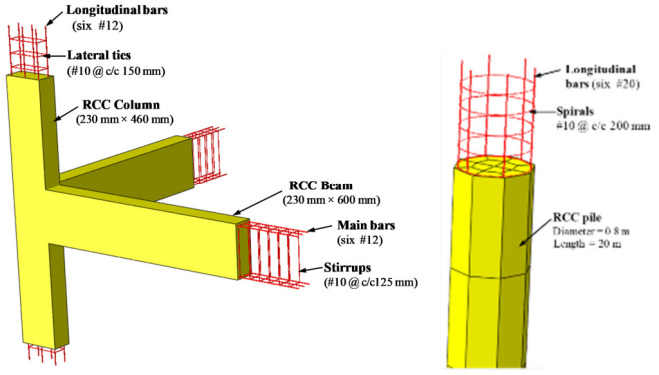

(a) (b)

Fig. 2. (a) Schematic illustration of a normal fault rupture interaction with a high-rise building, (b) pile arrangement in the raft.

C. Features of the Foundation

The building was founded on a 15m size and 1.5m thickness square raft supported by a group of piles in a 4×4 configuration with center to center distance of 3.75m (Figure 1(b)). The diameter (d_p) and length (L_p) of each pile were 0.8m and 20m, respectively. Figure 2(b) shows the section of a

typical pile with reinforcement. The pile is reinforced with six 20mm diameter longitudinal bars which are equally spaced around the pile. These bars are connected with spirals of 10mm diameter with center to center spacing of 200mm.

D. Characteristics of the Numerical Model

Figure 3 shows the finite element mesh developed in Abaqus software. The size of the mesh numerical run was taken as 120m×60m×30m. The different structural components of the building frame (i.e. beams and columns) and the slabs and raft were modelled by eight-node hexahedral brick elements (C3D8) and four-node shell elements (S4), respectively. The concrete damaged plasticity constitutive model is based on the fracture energy theory and the plastic-damage model of [11] is adopted to simulate the nonlinear behavior of the building frame. Elastic perfectly-plastic constitutive model is used to model the mechanical behavior of steel reinforcements. The detailed steel reinforcement and concrete material properties are listed in Table I. Eight-node hexahedral brick (C3D8) elements were used to model the soil and the piles, while two-node truss elements were adopted to model the steel reinforcements of beams, columns and piles. The size of the elements was chosen as 1.5mm.

TABLE I. MECHANICAL PROPERTIES OF THE FRAME OF THE BUILDING

Material	Constitutive model	Input parameter	Value
Concrete	Damage plasticity model	Mass density (kg/m^3)	2400
		Elastic Modulus (kPa)	3.15×10^7
		Poisson's ratio (v)	0.2
		Dilation angle (°)	30
		Eccentricity	0.1
		Stress ratio	0.666
		Ultimate strength ratio	1.16
		Tensile yield stress (kPa)	1.32×10^3
		Compressive yield stress (kPa)	6.17×10^3
Steel reinforcement	Elastic-perfectly-plastic	Mass density (kg/m^3)	7850
		Elastic Modulus (kPa)	2000
		Poisson's ratio (v)	0.3
		Yield stress (kPa)	4×10^5

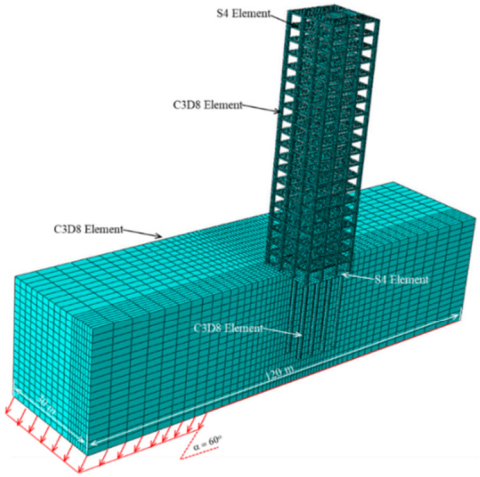

Fig. 3. 3D finite element mesh (showing the building and the foundation).

Since the stress-strain relationship of soils is highly nonlinear even at very small strain and the stiffness of the soil depends on the recent stress or strain history of the soil [12], an advanced hypoplastic model was used in this study to simulate the behavior of sand. The basic hypoplastic soil model requires 8 material parameters to describe the non-linear behavior of the sand (ϕ'_c, h_s, n, e_{d0}, e_{c0}, e_{i0}, α and β). Parameter ϕ'_c is soil frictional angle at the critical state. Parameters h_s and n are used to describe the shape of limiting void ratio lines. Parameters e_{d0}, e_{c0}, and e_{i0} are reference void ratios of isotropic normal compression line, critical state line, and minimum void ratio line, respectively. The effects of soil relative density on peak frictional angle and shear stiffness are characterised by α and β. To consider the small strain stiffness and stress path-dependent soil behavior, the concept of intergranular strain is incorporated into the basic model [13], which includes additional five parameters (m_R, m_T, R, β_r and χ). By using the concept of intergranular strain, the modified hypoplastic sand model has the ability to capture effects of shear strain and stress path on soil stiffness. These five parameters were obtained by fitting the stiffness degradation curves of Toyoura sand obtained from the stress-path triaxial tests carried out in [11]. The model parameters were taken from [14]. The authors calibrated and validated all the parameters of the hypoplastic sand model against their centrifuge test results (which was performed to simulate excavation in sand). These parameters are summarized in Table II.

TABLE II. HYPOPLASTIC MODEL PARAMETERS OF SAND

Description	Parameter
Effective angle of shearing resistance at critical state: ϕ'c	31°
Hardness of granulates, hs	2.6GPa
Exponent n	0.27
Minimum void ratio at zero pressure, e_{d0}	0.61
Maximum void ratio at zero pressure, e_{c0}	1.10
Critical void ratio at zero pressure, e_{i0}	0.98
Exponent α	0.14
Exponent β	6
Parameter controlling initial shear modulus upon 180° strain path reversal, m_R	11
Parameter controlling initial shear modulus upon 90° strain path reversal, m_T	6
Size of elastic range, R	2×10^{-5}
Parameter controlling degradation rate of stiffness with strain β_r	0.1
Parameter controlling degradation rate of stiffness with strain χ	1.0

The lateral coefficient of earth pressure (K_0) is estimated by the empirical equation $(1-\sin\varphi')$ proposed in [15], where φ' is the internal friction of soil at the critical state. Since the internal friction angle of Toyoura sand at the critical state is 31°, thus, the K_0 value is estimated as 0.5.

E. Soil Structure Interactions and Boundary Conditions

When modeling the excavation-pile-soil problem, one of the most important aspects of modeling Soil Structure Interaction (SSI) is to establish the interaction between the pile and the surrounding soil, because relative pile soil movement and separation between the raft and the soil can occur during the propagation of the normal fault rupture. To incorporate the interactions between pile-soil and raft-soil, surface-to-surface contact technique provided in Abaqus software package was

used. The interface was modeled by the Coulomb friction law, in which the interface friction coefficient (μ) and limiting displacement (γ_{lim}) are required as input parameters. A limiting shear displacement of 5mm was assumed to achieve full mobilization of the interface friction equal to μ×p', where p' is the normal effective stress between two contact surfaces, and a typical value 0.35 of μ for a bored pile was used in all analyses [14]. Roller and pin supports were applied to the vertical sides and the base of the mesh, respectively. Therefore, the movements normal to the vertical boundaries and in all directions of the base were restrained.

F. Fault Simulation

Since the primary goal of this study is the interactive mechanism between the fault rupture and the foundation, the bedrock was simulated as a rigid boundary. To model fault rupturing in the bedrock, the bottom boundary which corresponded to the surface of the bedrock was split into two parts, as shown in Figure. 3. The left part represented the hanging wall (i.e. the moving block), and the other part simulated the footwall. As Figure 3 shows, during the fault rupturing the boundaries of the hanging wall (i.e. the moving block) moved downwards parallel to the dip angle (i.e. α = 60°). Note that in order to satisfy the equilibrium, the bottom and left boundaries of the hanging block were subjected to displacement to simulate fault rupturing.

G. Numerical Simulation Procedure

Numerical simulations of three cases were carried out in the following steps:

- Step 1: Initial geostatic stresses were generated in the mesh by applying gravity load. The considered coefficient of lateral earth pressure was 0.5.
- Step 2: The piles were constructed and the raft was placed on the top of the pile group and soil deposit.
- Step 3: The 20-story building was constructed on top of the pile raft. A live load of 5kPa was applied on the floor slab of each story.

Displacements were applied to the base and side boundaries of the hanging wall to simulate a fault rupture in the rock layer beneath, with a dip of 60° (as shown in Figure 3).

III. INTERPRETATION OF COMPUTED RESULTS

A. Evolution of Differential Settlement of the Piled Raft with Propagation of the Fault Rupture

Figure 4 shows the differential settlement (between point A and point B, see the inset) with propagation of the fault slip (h) which has an outcrop to the right (s/B=−1.0), mid (s/B=0.5), and left (s/B=2.0) of the raft. The positive and negative values of the differential settlement represent the tilting of the building towards the hanging wall and the footing wall, respectively. It can be seen from the Figure that the induced differential settlement increased as the fault rupture propagated in all cases. However, no further increment in the differential settlement was induced as the fault rupture increased beyond 0.15m when s/B=−1.0, because the location of the outcrop of the fault rupture at the ground surface in that case is 15m away from the left pile (discussed in section A), hence the piled raft is within the (stationary) footwall and further increase of the fault rupture height did not increase the height of the fault slope. On the other hand, the differential settlement kept increasing when s/B=0.5. This can be attributed to the outcrop of the fault rupture which crossed the middle of the piled raft and, as a result, the intensive shear zone due to the fault rupture passed through the middle of the raft (as discussed above). Therefore, the movement of the hanging (moving) wall tended to pull down the piles located to the left of the piled raft middle whereas the piles right to the piled raft middle were fixed within the (stationary) footwall. This results in the maximum differential settlement when s/B=0.5. Consequently, substantial counter clockwise rotation of the piled raft (hence building) was induced. The resulting differential settlement caused the distress not only in the RCC frame of the building but also in the pile head accompanied by the extensive yielding in reinforcement of the frame (also discussed above). In addition, significant shear force and bending moment were developed in the piles. In contrast to the two previous discussed cases (s/B=−1.0, 0.5), negative differential settlement was induced as the fault rupture propagated beyond 0.15m for s/B= 2.0, because the rupture crossed the toe of the right piles and outcrop away from the piled raft and the location of the outcrop of the fault rupture at the ground surface in this case is 15m away from the right pile, hence the piled raft is within the hanging (moving) wall. Consequently, the piles located at the right side of the piled raft were subjected to intensive shear strain. This led the piled raft to rotate clockwise (induced negative differential settlement). Among the three simulated cases, the maximum differential settlement occurred for s/B=0.5. The final computed differential settlement values were 14, 48, and −9mm for s/B=−1.0, 0.5, and 2.0, respectively.

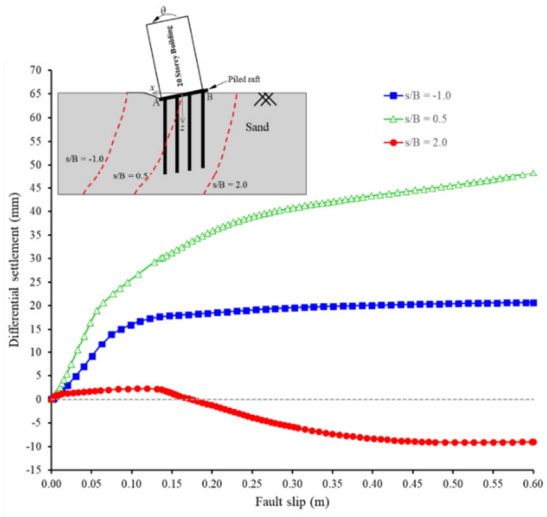

Fig. 4. Induced piled raft settlement during the propagation of the fault rupture.

B. Induced Lateral Displacement of the High-rise Building

Figure 5 illustrates the lateral movement of each floor of the building after the occurrence of the fault rupture for s/B=−1.0, 0.5, and 2.0. The general trend of the lateral deflection profile

is consistent with differential settlement. It can be seen that the lateral movement of each floor is larger than that of its bottom floor when s/B=−1.0, 0.5. The maximum lateral deflection occurred at the top of the building (the roof level of the 20th story), because the location of the outcrop of the fault rupture at the ground surface for s/B=−1.0 is 15m away from the left pile, hence the piled raft is within the (stationary) footwall and further increase of the fault rupture height did not increase the height of the fault slope. Therefore, the movement of the hanging (moving) wall tended to pull down the piles located to the left of the piled raft middle whereas the piles right to the piled raft middle were fixed within the (stationary) footwall, resulting in lateral movement of the building. Consequently, substantial counter clockwise rotation of the piled raft (hence building) was induced. The resulting lateral movement caused the distress not only in the RCC frame of the building but also in the pile head accompanied by the extensive yielding in the reinforcement of the frame.

In contrast to the two cases discussed above (s/B=−1.0, 0.5), the lateral movement of each floor is smaller than that of its bottom floor when s/B=2.0. Moreover, the largest lateral movement was induced, due to the rupture that crossed the toe of the right piles and the outcrop away from the piled raft. The location of the outcrop of the fault rupture at the ground surface for s/B= 2.0 is 15m away from the right pile hence the piled raft is within the hanging (moving) wall. Consequently, the piles located at the right side of the piled raft were subjected to intensive shear strains zone. This led the piled raft to rotate clockwise (induced lateral movement). Among the three simulated cases, the maximum lateral movement values in the 20th floor of the building for s/B=−1.0, 0.5, and 2.0 were computed as 100, 270, and 260mm, respectively. In each case, the lateral movement of the building due to the occurrence of the fault rupture caused inter-story drift which may induce distress in the structural components of the building. The inter-story drift of the building can be defined as the ratio of difference of deflections of two storys to story height.

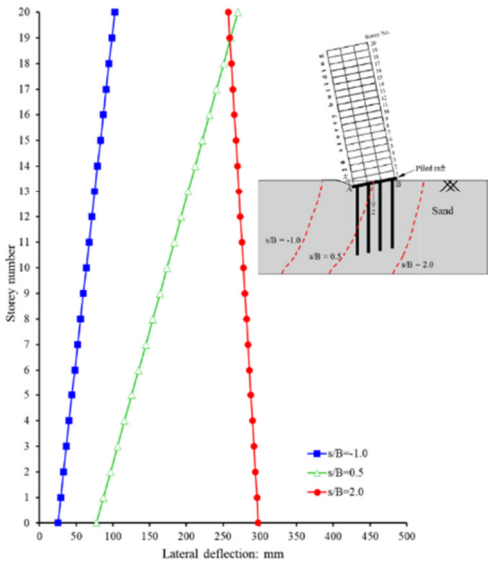

Fig. 5. Induced lateral displacement.

C. *Evolution of Damage (Damage Indices) in the Frame of the Building during the Occurrence of Fault Ruptures*

The induced differential settlement and the lateral deflection of the building due to twin excavation can generate substantial plastic strains which can cause cracks in the building. As discussed above, the nonlinear (elasto-plastic) concrete behavior is simulated with a concrete damage plasticity model. In that model, compressive and tensile damage indices (DAMAGEC and DAMAGET, respectively) range between 0 (no damage) and 1 (full damage). It was observed from the software output that both types of damage occurred only in the beams and the columns of the first story of the building. Therefore, the key locations were selected in the beams and the columns (see inset in Figure 6) to investigate the evolution of the damage during the occurrence of the fault rupture. Figure 6 shows the tensile damage index in the selected locations during the occurrence of fault rupture for s/B=−1.0, 0.5, and 2.0.

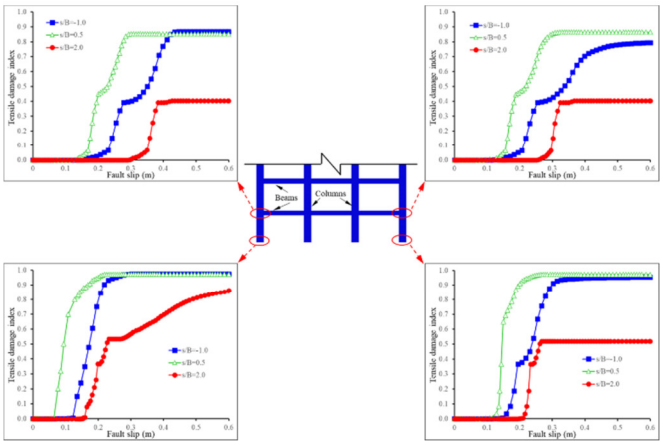

Fig. 6. Tensile damage in beams and columns.

In Figure 6, it can be observed that the beams and the columns at the selected locations were fully damaged in tension when s/B=−1.0, 0.5. However, the damage evolved earlier when s/B=−1.0 than when s/B=0.5. The resulting tensile damage occurred due to the substantial induced differential settlement (see Figure 4) and the lateral movement of the frame (see Figure 5). The induced differential settlement induced additional bending moment at the first story of the building. Because the frame of the building was rigidly connected to the raft, the additional bending moment resulted in tensile damages at the bottom of the column and both the left and right ends of the beam of the first story of the building. In contrast, the magnitude of tensile damage in the frame when s/B=2.0 was smaller than that for s/B=−1.0 and 0.5, due to the smaller differential settlement induced to the fault rupture and the rupture crossed the toe of the right piles and outcrop away from the piled raft. The location of the outcrop of the fault rupture at the ground surface for s/B=2.0 is 15m away from the right pile, hence the piled raft is within the hanging (moving) wall. Consequently, the piles located at the right side of the piled raft were subjected to intensive shear strains. This led the piled raft to rotate clockwise (induced negative differential settlement).

The magnitudes of maximum tensile damage at each location were computed as 1.when s/B=−1.0 and 0.5, impying that the building failed in both these cases.

In addition to tensile cracks developed in the frame of the building, crushing of the concrete at the base of the columns of the first story of the building occurs. The crushing of the concrete is expressed in terms of compressive index (DAMAGEC). Figure 7 shows the compressive damage index in at the base of the column (connection point between the raft and the column) during the occurrence of the fault rupture when s/B=−1.0, 0.5, and 2.0. Similar to tensile damage index, the compressive indices are larger when s/B=−1.0, 0.5 than when s/B=2.0. However, the development of crushing of the concrete initiated the fault rupture increased beyond 0.3m in every case. The concrete crushing resulted due to the additional bending moment due to the differential settlement of the building. The resulting additional bending moment due to the fault rupture induced stress in the concrete at the base of the column. The magnitudes of the compressive damage (0.4) are much less than that of the magnitude of full damage (1.0), implying that the failure of the frame occurred due to tensile cracks at the base of the frame.

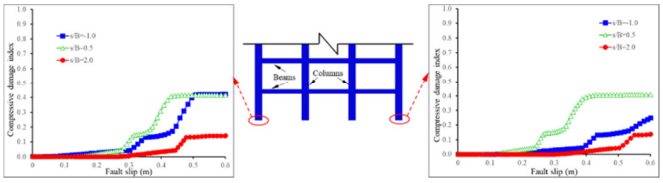

Fig. 7. Compressive damage in columns.

IV. CONCLUSIONS

Based on sand density and the high-rise building geometry, the following conclusions can be drawn:

- The performance of the building due to the propagation of the normal fault rupture depends on the position of the outcrop of the rupture with respect to the building.
- Among the three simulated cases, the maximum differential settlement occurred when s/B=0.5. This can be attributed to the outcrop of the fault rupture which crossed the middle of the piled raft and as a result the intensive shear zone due to the fault rupture passed through the middle of the raft. Therefore, the movement of the hanging (moving) wall tended to pull down the piles located to the left of the piled raft middle whereas the piles at the right of the piled raft middle were fixed within the (stationary) footwall.
- In contrast to s/B=−1.0, 0.5, negative differential settlement was induced as the fault rupture propagated beyond 0.15m when s/B=2.0 because the rupture crossing the toe of the right piles and the location of the outcrop of the fault rupture at the ground surface for s/B=2.0 was 15m away from the right pile, hence the piled raft was within the hanging (moving) wall.
- The lateral movement of each floor is larger than that of its bottom floor when s/B=−1.0 and 0.5. The maximum lateral deflection occurred at the top of the building (the roof level of the 20th store). In every case, the lateral movement of the building caused inter-story drift which may induce stress in the structural components of the building.
- The beams and the columns of the first story were fully damaged in tension when s/B=−1.0, 0.5. In contrast the magnitude of tensile damage in the frame when s/B=2.0 was smaller.
- In addition to tensile cracks developing in the frame of the building, concrete crushing occurred at the base of the columns of the first story of the building.

REFERENCES

[1] M. Loli, M. f. Bransby, I. Anastasopoulos, and G. Gazetas, "Interaction of caisson foundations with a seismically rupturing normal fault: centrifuge testing versus numerical simulation," *Géotechnique*, vol. 62, no. 1, pp. 29–43, Jan. 2012, https://doi.org/10.1680/geot.9.P.153.

[2] M. F. Bransby, M. C. R. Davies, and A. El. Nahas, "Centrifuge modelling of normal fault–foundation interaction," *Bulletin of Earthquake Engineering*, vol. 6, no. 4, pp. 585–605, Nov. 2008, https://doi.org/10.1007/s10518-008-9079-0.

[3] J. Shi *et al.*, "Effects of construction sequence of double basement excavations on an existing floating pile," *Tunnelling and Underground Space Technology*, vol. 119, Jan. 2022, Art. no. 104230, https://doi.org/10.1016/j.tust.2021.104230.

[4] J. Wang, G. Ma, H. Zhuang, Y. Dou, and J. Fu, "Influence of diaphragm wall on seismic responses of large unequal-span subway station in liquefiable soils," *Tunnelling and Underground Space Technology*, vol. 91, Sep. 2019, Art. no. 102988, https://doi.org/10.1016/j.tust.2019.05.018.

[5] M. A. Soomro, K. F. Memon, M. A. Soomro, A. Memon, and M. A. Keerio, "Single Pile Settlement and Load Transfer Mechanism due to Excavation in Silty Clay," *Engineering, Technology & Applied Science Research*, vol. 8, no. 1, pp. 2485–2492, Feb. 2018, https://doi.org/10.48084/etasr.1666.

[6] M. F. Bransby, M. C. R. Davies, A. El Nahas, and S. Nagaoka, "Centrifuge modelling of reverse fault–foundation interaction," *Bulletin of Earthquake Engineering*, vol. 6, no. 4, pp. 607–628, Nov. 2008, https://doi.org/10.1007/s10518-008-9080-7.

[7] N. Mangi, D. A. Mangnejo, H. Karira, M. Kumar, A. A. Jhatial, and F. R. Lakhair, "Crack Pattern Investigation in the Structural Members of a Framed Two-Floor Building due to Excavation-Induced Ground Movement," *Engineering, Technology & Applied Science Research*, vol. 9, no. 4, pp. 4463–4468, Aug. 2019, https://doi.org/10.48084/etasr.2923.

[8] A. Behshad and M. R. Shekari, "Seismic Performance Evaluation of Concrete Gravity Dams with Penetrated Cracks Considering Fluid–Structure Interaction," *Engineering, Technology & Applied Science Research*, vol. 8, no. 1, pp. 2546–2554, Feb. 2018, https://doi.org/10.48084/etasr.1729.

[9] C. W. W. Ng, M. Shakeel, J. Wei, and S. Lin, "Performance of Existing Piled Raft and Pile Group due to Adjacent Multipropped Excavation: 3D Centrifuge and Numerical Modeling," *Journal of Geotechnical and Geoenvironmental Engineering*, vol. 147, no. 4, Apr. 2021, Art. no. 04021012, https://doi.org/10.1061/(ASCE)GT.1943-5606.0002501.

[10] E. Faccioli, I. Anastasopoulos, G. Gazetas, A. Callerio, and R. Paolucci, "Fault rupture–foundation interaction: selected case histories," *Bulletin of Earthquake Engineering*, vol. 6, no. 4, pp. 557–583, Nov. 2008, https://doi.org/10.1007/s10518-008-9089-y.

[11] A. W. Skempton and D. H. Macdonald, "The allowable settlements of buildings.," *Proceedings of the Institution of Civil Engineers*, vol. 5, no. 6, pp. 727–768, Nov. 1956, https://doi.org/10.1680/ipeds.1956.12202.

[12] I. Anastasopoulos, G. Gazetas, V. Drosos, T. Georgarakos, and R. Kourkoulis, "Design of bridges against large tectonic deformation," *Earthquake Engineering and Engineering Vibration*, vol. 7, no. 4, pp. 345–368, Dec. 2008, https://doi.org/10.1007/s11803-008-1001-x.

[13] A. Niemunis and I. Herle, "Hypoplastic model for cohesionless soils with elastic strain range," *Mechanics of Cohesive-frictional Materials*, vol. 2, no. 4, pp. 279–299, 1997, https://doi.org/10.1002/(SICI)1099-1484(199710)2:4<279::AID-CFM29>3.0.CO;2-8.

[14] J. Jaky, "The coefficient of earth pressure at rest," *Journal of the Society of Hungarian Architects and Engineers*, pp. 355–358, 1944.

[15] J. Lubliner, J. Oliver, S. Oller, and E. Oñate, "A plastic-damage model for concrete," *International Journal of Solids and Structures*, vol. 25, no. 3, pp. 299–326, Jan. 1989, https://doi.org/10.1016/0020-7683(89)90050-4.